Journal of Molecular Structure 1079 (2015) 194–202

Contents lists available at ScienceDirect

Journal of Molecular Structure

journal homepage: www.elsevier.com/locate/molstruc

FT-IR and Raman vibrational analysis, B3LYP and M06-2X simulations of 4-bromomethyl-6-tert-butyl-2H-chromen-2-one

Yusuf Sert [a,b,*], K.B. Puttaraju [c], Sema Keskinoğlu [a], K. Shivashankar [c], Fatih Ucun [d]

[a] Department of Physics, Faculty of Art & Sciences, Bozok University, Yozgat 66100, Turkey
[b] Sorgun Vocational School, Bozok University, Yozgat 66100, Turkey
[c] P.G. Department of Chemistry, Central College Campus, Bangalore University, Bangalore 560 001, India
[d] Department of Physics, Faculty of Art & Sciences, Suleyman Demirel University, Isparta 32100, Turkey

HIGHLIGHTS

- The FT-IR and Raman spectra of the title compound were recorded in solid phase.
- The optimized geometry and vibrational frequencies were calculated for the first time.
- The complete assignments are performed on the basis of the potential energy distribution (PED).
- The HOMO–LUMO energies and related molecular properties were evaluated.

GRAPHICAL ABSTRACT

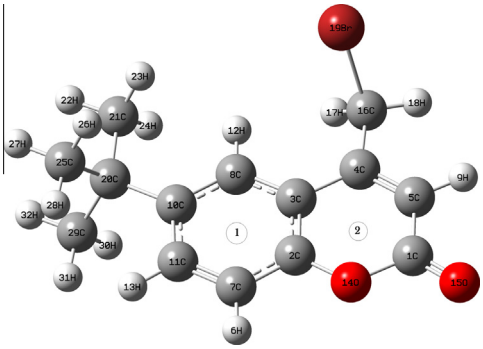

ARTICLE INFO

Article history:
Received 11 August 2014
Received in revised form 11 September 2014
Accepted 12 September 2014
Available online 20 September 2014

Keywords:
FT-IR
Raman
DFT
Coumarin

ABSTRACT

In this study, the experimental and theoretical vibrational frequencies of a newly synthesized bacteriostatic and anti-tumor molecule namely, 4-bromomethyl-6-tert-butyl-2H-chromen-2-one have been investigated. The experimental FT-IR (4000–400 cm^{-1}) and Raman spectra (4000–100 cm^{-1}) of the compound in solid phase have been recorded. The theoretical vibrational frequencies and optimized geometric parameters have been calculated using density functional theory (DFT/B3LYP: Becke, 3-parameter, Lee-Yang-Parr and DFT/M06-2X: highly parametrized, empirical exchange correlation function) with 6-311++G(d, p) basis set by Gaussian 03 software, for the first time. The assignments of the vibrational frequencies have been done by potential energy distribution (PED) analysis using VEDA 4 software. The theoretical optimized geometric parameters and vibrational frequencies have been found to be in good agreement with the corresponding experimental data and results in the literature. In addition, the highest occupied molecular orbital (HOMO) energy, the lowest unoccupied molecular orbital (LUMO) energy and the other related molecular energy values of the compound have been investigated using the same theoretical calculations.

Introduction

Coumarins are important oxygen containing fused heterocycles, and found abundantly in numerous naturally occurring products, including edible vegetables and fruits [1]. They are used as additives in food and cosmetics, optical brightening agents and

* Corresponding author at: Department of Physics, Faculty of Art & Sciences, Bozok University, Yozgat 66100, Turkey. Tel.: +90 354 2421021; fax: +90 354 2421022.
E-mail address: yusufsert1984@gmail.com (Y. Sert).

http://dx.doi.org/10.1016/j.molstruc.2014.09.043
0022-2860/

dispersed fluorescent and laser dyes [2]. The coumarin derivatives exhibit a remarkable array of biochemical and pharmacological actions, such as anti-fungal, antihypertensive, antioxidant and antimicrobial activity [3–8]. Some of the coumarin derivatives are also reported as chemotherapeutic agents [9–12]. There has been, in recent years, a major rekindling of interest in the studies on the defensive effects of coumarins as antioxidants [13,14]. In the literature, some coumarin derivatives have been reported to inhibit most potent antiinflammatory activity [15,16]. Further studies have shown some plant derived coumarins to inhibit the activation of NF–kB [17]. It is therefore of utmost importance that the synthesis of coumarins should be achieved by a simple and effective method. The Pechmann reaction for the synthesis of coumarin involves the condensation of phenols with β-ketonic esters in the presence of acidic condensing agent [18].

The structure of the title compound, 4-bromomethyl-6-tert-butyl-2H-chromen-2-one, has been studied by single crystal X-ray spectroscopy [19]. Although X-ray diffraction method is one of the most frequently applied techniques for structural characterization of pharmaceutical compounds but the use of vibrational spectroscopy is also gaining increasing attention. X-ray diffraction technique is sensible to the long range order while vibrational spectroscopy (IR and Raman) is applicable to the short-range structure of molecular solids. As the literature survey reveals neither Raman and IR spectra nor quantum chemical calculations of the compound have been reported, so far, hence the present work was undertaken to study the vibrational spectra of the compound with together quantum chemical calculations. We have interpreted the calculated spectra in terms of potential energy distribution (PED).

Experimental details

FT-IR spectrum (4000–400 cm^{-1}) of 4-bromomethyl-6-tert-butyl-2H-chromen-2-one has been recorded by Perkin–Elmer Spectrum Two FT-IR Spectrometer with a resolution of 4 cm^{-1} in solid phase at room temperature. The Raman spectrum has been recorded on Renishaw Invia Raman microscope spectrophotometer in the 4000–100 cm^{-1} region. The excitation line at 785 nm has been taken from a diode laser. Its scan number is 100, the resolution is 1 cm^{-1} and the sample is in solid phase, however some peaks could not be observed due to fluorescence. So, identified peaks have been taken in Raman spectrum.

Computational details

Density functional theory (DFT) is an approach to the electronic structure of atom and molecules, and states that all the ground-state properties of a system are function of the charge density. So, DFT calculations cannot be considered a pure *ab initio* method. In DFT, the electron density is the basic variable instead of the wave function. This reduces the computational burden of electron–electron interaction terms which are taken explicitly as a functional of the density. So, DFT approach combines the capacity to incorporate exchange-correlation effects of electrons with reasonable computational costs and high accuracy. Therefore in the past few years has been seen a rapid increase in the use of DFT methods in different types of applications, particularly since of the introduction of accurate non-local corrections. In DFT, since the exchange-correlation energy is the main issue among of all the approximations, its accuracy is depended directly on the approximate nature of the exchange-correlation energy functional. The DFT methods employed in the present paper are representative in aspect of the exchange–correlation energy, which is commonly used in numerous theoretical studies.

The high parameterized empirical exchange correlation functionals, M05-2X and M06-2X which are developed by Zhao and Truhlar [20], have been used to describe noncovalent interactions better than density functionals being currently in common use. However, these methods have not yet to be fully benchmarked for the types of interactions which are important in biomolecules. M05-2X and M06-2X are claimed to capture "medium-range" electron correlation; however, the "long-range" electron correlation neglected by these functionals can also be important in the binding of noncovalent complex.

Initial atomic coordinates can be generally taken from any database or experimental XRD results. We have also used the experimental XRD data and GaussView software database to determine initial atomic coordinates, and to optimize the input structure. After the optimization the most stable optimized structure was obtained and, used for other theoretical analysis.

The molecular structure of the title molecule in the ground state (in gas phase) has been optimized by using DFT/B3LYP and M06-2X methods with 6-311++G(d,p) basis set level. And the calculated optimized structure has been used in the vibrational frequency calculations. The calculated harmonic vibrational frequencies have been scaled by 0.9614 (B3LYP) and 0.9489 (M06-2X) for 6-311++G(d,p) level, respectively [21,22]. The same scale factors were used for the entire spectra. The molecular geometry has not been limited, and all the calculations (vibrational wavenumbers, optimized geometric parameters and other molecular properties) have been performed using the Gauss View molecular visualization program [21] and the Gaussian 03 software package on a computing system [23]. Furthermore, the calculated vibrational frequencies have been clarified by means of the potential energy distribution (PED) analysis of all the fundamental vibration modes by using VEDA 4 program [24,25]. VEDA 4 program has been used in previous studies by many researchers. All the vibrational assignments have been made at B3LYP/6-311++G(d,p) level for which the molecular structure is more stable. So, some assignments may correspond to its previous or next vibrational frequency value at M06-2X/6-311++G(d,p) level.

Results and discussion

Geometric structure

The single X-ray crystallographic analysis of the title compound ($C_{14}H_{15}BrO_2$) shows that its crystal possesses space $P2_1/c$, and belongs to monoclinic system with the following cell dimensions: a = 10.3311 Å, b = 16.830 Å, c = 7.3374 Å and, β = 97.518° and V = 1264.8 $Å^3$ [19]. In the compound, the coumarin ring is substituted with bromomethyl group at C4 and tert-butyl group at C10. The comarin ring is assentialy planar. Among the three methyl groups belonging to tert-butyl moiety two methyl groups, C25 and C29, deviate from the plane of the coumarin ring whereas the carbon atom C21 of the methyl group lies within the plane, and in the crystal structure of the compound, weak C—H···O interactions link the molecules into zigzag chains extending along the c-axis direction. These chains are further assembled into (1 0 0) layers via π–π stacking interactions between inversion-related chromenone fragments [interplanar distance is 3.376 Å]. The measured density is 1.550 mg/m^3 [19]. The theoretical and experimental structure parameters (bond lengths, bond angles and torsion angles) are shown in Table S1 (Supporting Information) in accordance with the atom numbering scheme in Fig. 1.

In the ring 1 and ring 2, the C11=C7 and C4=C5 bond lengths have been calculated as 1.384(B3LYP)/1.381(M06-2X) and 1.356(B3LYP)/1.346(M06-2X) Å, respectively. These bond lengths have experimentally been found as 1.378 and 1.356 Å, respectively

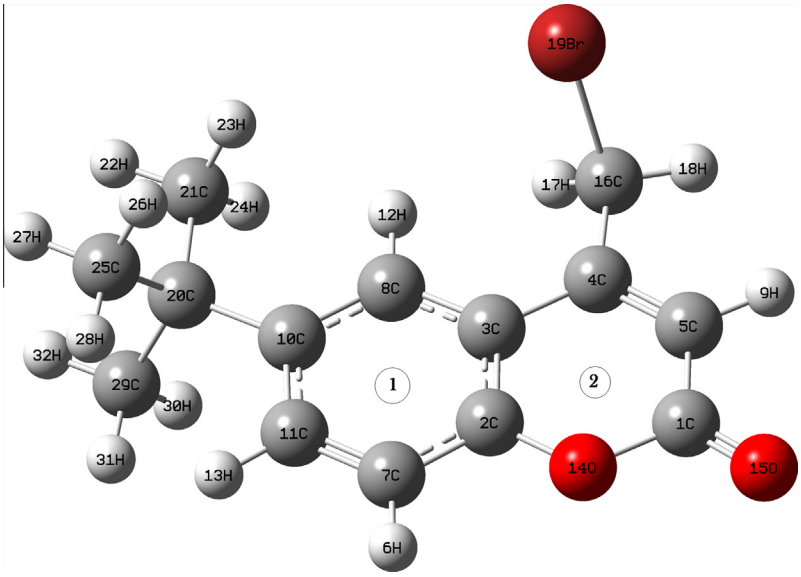

Fig. 1. The optimized molecular structure of the title compound.

[19]. For 6-methoxy-4-methyl-2H-chromen-2-one these bond lengths have been identified as 1.370 and 1.348 Å, respectively by Fun et al. [26]. For 4-bromomethyl-6-methoxy-2H-chromen-2-one these bonds have been reported at 1.382 and 1.459 Å, respectively by Gowda et al. [27]. In bromomethyl group the C16—Br19 bond length has been calculated at 1.996(B3LYP)/1.963(M06-2X) Å. This bond length has experimentally been found at 1.957 Å [19]. By Gowda et al. [27] the C16—Br19 bond has been reported at 1.950 Å for 4-bromomethyl-6-methoxy-2H-chromen-2-one. By Sortur et al. [28], C16—Br19 bond length has been calculated as 1.963 and 1.994 Å by using RHF and RB3LYP with 6-31G* basis set, respectively, and has been reported at 1.962 Å as experimentally. Similarly, the C16—Br19 bond have been calculated at 1.991(RB3LYP)/1.961(RHF) Å with 6-31G* for monomeric 6-chloro- and 7-chloro-4-bromomethylcoumarins by Tonannavar et al. [29]. In ring 1 and ring 2 (chromene group) C2—O14, C1—O14 and C1=O15 bond lengths have been calculated at 1.366(B3LYP)/1.362(M06-2X) Å, 1.389(B3LYP)/1.373(M06-2X) Å and 1.204(B3LYP)/1.196(M06-2X) Å, respectively. These bond lengths have been given 1.387, 1.379 and 1.209 Å, respectively as experimentally. For 6-methoxy-4-methyl-2H-chromen-2-one these bond lengths have been identified as 1.381, 1.377 and 1.206 Å, respectively by Fun et al. [26]. For 4-bromomethyl-6-methoxy-2H-chromen-2-one these bonds have been reported at 1.377, 1.367 and 1.211 Å, respectively by Gowda et al. [27].

The C4—C16—Br19, O14—C1=O15 and C1—O14—C2 bond angles have been calculated at 112.2(B3LYP)/111.3(M06-2X), 118.3(B3LYP)/118.7(M06-2X) and 122.4(B3LYP)/122.4(M06-2X)° and these bond angles have experimentally been found as 110.7, 116.8 and 121.6°, respectively [19]. For 4-bromomethyl-6-methoxy-2H-chromen-2-one these bond angles have been identified as 112.1, 116.7 and 121.6°, respectively by Gowda et al. [27]. By Sortur et al. [28] these bond angles have been calculated at 112.2(RB3LYP)/111.2(RHF), 118.2(RB3LYP)/119.2(RHF) and 122.5(RB3LYP)/123.4(RHF)° by using 6-31G* basis set, respectively, and have been reported at 113.0, 117.0 and 122.1° as experimentally in this study. Similarly, these angles have been calculated at 112.1(RB3LYP)/112.1(RHF), 118.3(RB3LYP)/119.3(RHF) and 122.4(RB3LYP)/123.3(RHF)° with 6-31G* for monomeric 6-chloro- and 7-chloro-4-bromomethylcoumarins by Tonannavar et al. [29]. Also, in this study dihedral angles have been calculated with B3LYP and M06-2X methods with 6-311++G(d,p). the calculated results are seen to be good agreements with the experimental data. These can be seen from Table S1 (Supporting Information). To compare the calculated results with the experimental data we present linear correlation coefficients (R^2) for linear regression analysis of the theoretical and experimental bond lengths and angles. These values are 0.9819 and 0.9835 for the bond lengths, 0.9237 and 0.9332 for the bond angles and 0.9993 and 0.9990 for the dihedral angles at B3LYP and M06-2X levels, respectively. These coefficients can be seen in the last line of Table S1 (Supporting Information). From these values it can easily be concluded that the geometric parameters (bond lenghts, bond angles) calculated by the DFT/M06-2X method with 6-311++G(d,p) basis set is much closer to the experimental ones. But for dihedral angles, DFT/B3LYP method is much closer to the experimental ones.

Vibrational analysis

The experimental FT-IR and Raman spectra of the title compound are compared with the theoretical spectra in Figs. 2 and 3, respectively. The scaled calculated harmonic vibrational frequencies at both B3LYP and M06-2X levels, observed vibrational frequencies, and detailed PED assignments are tabulated in Table 1. Harmonic frequencies are calculated for gas phase of an isolated compound although experimental ones are obtained for its solid phase. Therefore there is disagreement between the observed and calculated frequencies in some modes. In order to introduce the detailed vibrational assignments of the compound the PED analysis has been carried out and given in Table 1. All the calculated modes are numbered from the largest to the smallest frequency within each fundamental wave number in the table.

C—CH_2 and C—Br vibrations

The CH_2 group has 6 vibrational modes (1 asymmetrical and 1 symmetrical stretching mode, 1 scissoring mode, 1 wagging mode, 1 twisting mode and 1 rocking mode). The asymmetric stretch $\nu_{as}CH_2$, symmetric stretch ν_sCH_2, scissoring vibrations δCH_2, and the wagging vibration ωCH_2 appear in the regions 3000 ± 20, 2900 ± 25, 1440 ± 10 and 1340 ± 25 cm^{-1}, respectively [30,31]. For our compound the CH_2 asymmetric stretching modes are observed at 3032 cm^{-1} in the FT-IR spectrum, but could not be detected in the Raman spectrum. This asymmetric stretching mode has been calculated at 3056(B3LYP)/3030(M06-2X) cm^{-1}. The CH_2

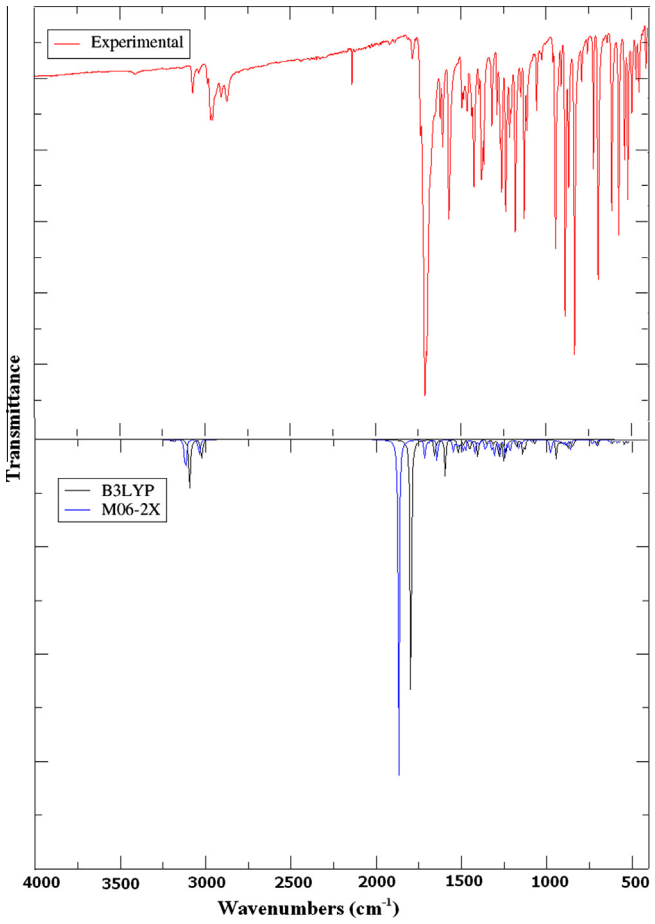

Fig. 2. Comparison of observed and calculated infrared spectra of the title compound.

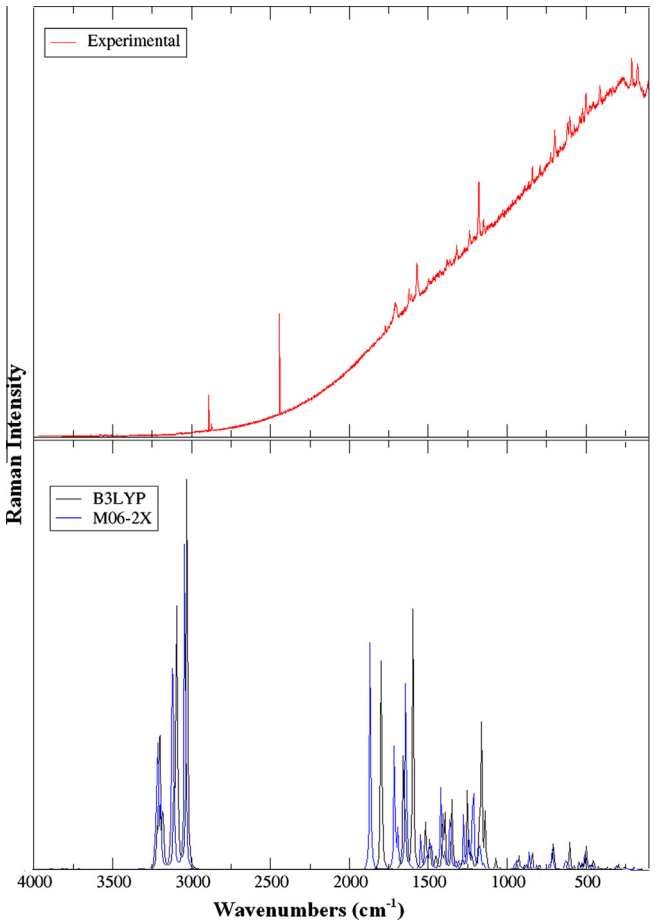

Fig. 3. Comparison of observed and calculated Raman spectra of the title compound.

symmetric stretching modes are not be observed in the FT-IR and Raman spectra. This symmetric stretching mode has been calculated at 2994(B3LYP)/2965(M06-2X) cm^{-1}. The CH_2 scissoring and wagging modes are observed at 1422(FT-IR) and 1317(FT-IR)/1322(Ra) cm^{-1}. These modes have been calculated 1421(B3LYP)/1411(M06-2X) and 1340(B3LYP)/1324(M06-2X) cm^{-1}. The CH_2 twisting and rocking modes appear in the regions 1260 ± 10 and 800 ± 25 cm^{-1} [30]. For the title compound, the CH_2 twisting and rocking modes are observed at 1261(FT-IR) and 832(FT-IR)/838(Ra) cm^{-1}. These modes have been calculated at 1264(B3LYP)/1257(M06-2X) and 843(B3LYP)/841(M06-2X) cm^{-1}, respectively. Also the other C—CH_2 modes are υC16—C4 stretching and δC16—C4—C5 bending modes. The υC16—C4 stretching mode has been observed at 1055 cm^{-1} in FT-IR spectrum and, calculated at 1030(B3LYP)/1031(M06-2X) cm^{-1}. The δC16—C4—C5 bending mode has been observed at 327 cm^{-1} in Raman spectrum and, calculated at 310(B3LYP)/332(M06-2X) cm^{-1}.

In the lower region, the C—Br stretching vibrations appear in the range 650–485 cm^{-1}[32–35] and the C—Br deformation vibrations in the region 300–140 cm^{-1} [32,33]. In this study the C—Br stretching modes have been observed at 574(FT-IR)/576(Ra), 521(FT-IR)/523(Ra), 472(FT-IR)/461(Ra) and 174(Ra) cm^{-1} in the experimental FT-IR and Ra spectra. These modes have been calculated at 579(B3LYP)/584(M06-2X), 524(B3LYP)/524(M06-2X), 480(B3LYP)/483(M06-2X) and 189(B3LYP)/187(M06-2X) cm^{-1}. Additionally, in this group the δBrCC and τBrCCC modes have been observed in the modes no: 83, 84, 87, 88 and 89, and given in Table 1. The other related modes are agreed with the literature.

Tert-Butyl Group vibrations

The 3-CH_3 group has 27 vibrational modes (6 asymmetrical and 3 symmetrical stretching modes, 6 antisymmetrical deformations, 3 symmetrical deformation, 6 rocking modes and 3 twisting mode). The CH_3 asymmetric stretching vibrations are expected in the range 2950–3050 cm^{-1} and the CH_3 symmetric vibrations in the range of 2900–2950 cm^{-1} [30,31]. For our molecule the asymmetric stretching modes of the methyl group are calculated at 2979(B3LYP)/2965(M06-2X), 2976(B3LYP)/2961(M06-2X), 2974-(B3LYP)/2959(M06-2X), 2971(B3LYP)/2958(M06-2X), 2967(B3LYP)/2953(M06-2X) and 2965(B3LYP)/2952(M06-2X) cm^{-1}, and the symmetric mode at 2913(B3LYP)/2887(M06-2X), 2906(B3LYP)/2882(M06-2X) and 2905(B3LYP)/2880(M06-2X) cm^{-1}. The asymmetric stretching modes have been observed at 2985 and 2966 cm^{-1} in the FT-IR spectrum, but these modes could not be seen in the Raman spectrum. The symmetric stretching mode has been observed at 2904 cm^{-1} in the FT-IR and 2894 cm^{-1} in the Raman spectra. Two bending can occur within a methyl group, the symmetrical bending vibration which involves in-phase bending of the C—H bonds and the asymmetrical bending vibration which involves out-of-phase bending of the C—H bonds. The asymmetrical deformations are expected in the range 1400–1485 cm^{-1} [30]. The calculated values of $\delta_{as}CH_3$ modes are at 1463(B3LYP)/1467(M06-2X), 1461(B3LYP)/1449(M06-2X), 1451(B3LYP)/1437-(M06-2X), 1447(B3LYP)/1430(M06-2X), 1434(B3LYP)/1416(M06-2X) and 1431(B3LYP)/1415(M06-2X) cm^{-1}. These bands have been observed at 1463 and 1435 cm^{-1} in the FT-IR, but these modes could not be seen in Raman spectrum. In many molecules, the

Table 1
Observed and calculated vibrational frequencies of title compound with 6-311++G(d,p).

Vibration no.	Assignments	Observed frequencies		Calculated frequencies in cm^{-1}	
		FT-IR	Ra	B3LYP	M06-2X
ν_1	υCH(98) in the R1	3073		3095	3066
ν_2	υCH(99) in the R2	3073		3080	3053
ν_3	υCH(98) in the R1	3073		3078	3047
ν_4	υCH(100) in the R1	3032		3060	3033
ν_5	υCH(98) in the CH2 as	3032		3056	3030
ν_6	υCH(98) in the CH2 s			2994	2965
ν_7	υCH(79) in the CH3 as	2985		2979	2965
ν_8	υCH(82) in the CH3 as	2966		2976	2961
ν_9	υCH(87) in the CH3 as	2966		2974	2959
ν_{10}	υCH(63) in the CH3 as	2966		2971	2958
ν_{11}	υCH(87) in the CH3 as	2966		2967	2953
ν_{12}	υCH(84) in the CH3 as	2966		2965	2952
ν_{13}	υCH(100) in the CH3 s	2904	2894	2913	2887
ν_{14}	υCH(96) in the CH3 s	2904	2894	2906	2882
ν_{15}	υCH(98) in the CH3 s	2904	2894	2905	2880
ν_{16}	υOC(85) in the O15—C1	1711	1708	1728	1772
ν_{17}	υCC(64) in the R1 and R2	1606	1627	1594	1627
ν_{18}	υCC(63) in the R1 and R2 + δHCC(13) R1 and R2	1570	1570	1583	1607
ν_{19}	υCC(29) in the R1 and R2 + δCCC(13) in the R1 + δHCC(12) in the R1 and R2	1570		1535	1558
ν_{20}	δHCH(31) in the CH3 asymm. Def.	1463		1463	1467
ν_{21}	δHCC(23) in the R1 + δHCH(16) in the CH3 asymm. Def.	1463		1461	1449
ν_{22}	δHCH(63) in the CH3 asymm. Def.+τHCCC(11) in the CH3 twisting mode	1435		1451	1437
ν_{23}	δHCH(59) in the CH3 asymm. Def.	1435		1447	1430
ν_{24}	δHCH(48) in the CH3 asymm. Def.	1435		1434	1416
ν_{25}	δHCH(45) in the CH3 asymm. Def.	1435		1431	1415
ν_{26}	δHCH(53) CH2 scissoring and CH3 twisting mode	1422		1430	1411
ν_{27}	δHCH(55) in the CH3 twisting mode	1422		1427	1406
ν_{28}	υCC(25) in the R1and R2	1394		1396	1403
ν_{29}	δHCH(86) in the CH3 symmet. def	1379	1378	1377	1359
ν_{30}	δHCH(16) in the CH3 symmet. def + δHCC(10) R1 and R2	1364	1369	1353	1349
ν_{31}	δHCH(81) in the CH3 symmet. def.	1364		1346	1328
ν_{32}	δHCH(14) in the CH2 wagging mode + υCC(11) in C3—C8 + δHCC(11) in R1and R2	1317	1322	1340	1324
ν_{33}	υCC(42) in the R1	1289		1297	1291
ν_{34}	δHCC(72) in the R1 and in the CH2 twisting mode	1261		1264	1257
ν_{35}	τHCCC(13) in the H22—C21—C20—C25 + υCC(10) in C10—C20 + δCCC(10) C21—C20—C29	1236	1240	1236	1243
ν_{36}	υOC(25) in the O14—C1 + δHCC(22) in the R1 and R2	1236	1240	1231	1238
ν_{37}	τHCCC(39) H17—C16—C4—C3 + δHCBr(11) H18—C16—Br19	1213	1211	1204	1210
ν_{38}	τHCCC(31) in the H17—C16—C4—C3 + δHCC(19) in the R2	1181	1178	1190	1181
ν_{39}	τHCCC(24) + υCC(13) in the C21—C20	1181	1178	1176	1180
ν_{40}	τHCCC(23) in the CH3 rocking mode + υCC(17) in the C25—C20	1181	1178	1174	1185
ν_{41}	δHCC(32) in the R1	1129	1149	1133	1153
ν_{42}	δHCBr(23) H18—C16—Br19 + υOC(10) in O14—C1	1113		1119	1116
ν_{43}	δHCBr(29) H18—C16—Br19 + υOC(15) in O14—C1 + τHCCC(10) in the CH3 rocking mode	1113		1096	1103
ν_{44}	δHCC(17) in the R1 + υOC(10) in O14—C1	1079		1085	1088
ν_{45}	υCC(29) in the C16—C4 + δCCC(17) in the R1	1055		1030	1031
ν_{46}	τHCCC(43) in the CH3 rocking mode	992		1008	998
ν_{47}	τHCCC(56) in the CH3 rocking mode	992		1000	992
ν_{48}	τHCCC(69) out of H in the R1	944		946	951
ν_{49}	τHCCC(37) in the CH3 rocking mode	930		923	927
ν_{50}	υOC(28) in the O14—C1 + δCCC(17) in the R1	912		907	910
ν_{51}	υCC(48) in the C10—C20 + τHCCC(11) in the CH3 rocking mode	912		902	904
ν_{52}	υCC(45) in C10—C20 + τHCCC(16)	888		891	896
ν_{53}	υCC(15) in C10—C20 + τHCCC(11)+δCCC(10) in the R1	888		887	889

v_{54}	τHCCC(89) in the R1 out of H	868		872	872
v_{55}	τHCCC(62) in the R2 out of H	868		857	857
v_{56}	τHCCC(28) in the CH2 rocking mode + δHCBr(11) H18—C16—Br19	832	838	843	841
v_{57}	τHCCC(68) in the R1 out of H	832		818	818
v_{58}	δCOC(18) in the C1—O14—C2 + υCC(14) in C21—C20 + δCCC(14) in the R2 C5—C4—C3	791	795	810	815
v_{59}	υCC(66) in C21—C20	758		764	768
v_{60}	τHCCC(19) in the R1 out of H + τCCCC(47) in the C5—C4—C3—C8 + γOCCC(10) O14—C7—C3—C2	723	728	731	715
v_{61}	γOCOC(68) O15—C1—O14—C2	695	700	691	695
v_{62}	δ CCC(18) in the R1 + γCCCC(10) in the R1 and R2	695	700	681	679
v_{63}	γCCCC(29) in the R1 and R2 + δCCC(10) in the R1	695	700	674	674
v_{64}	υCC(15) in C10—C20 + υOC(14) in O 14—C1	614	614	591	599
v_{65}	υBrC(19) in Br 19—C16 + γCCCC(17) in the R1 and R2	574	576	579	584
v_{66}	δOCO(30) in the O15—C1—O14	539	542	554	556
v_{67}	υBrC(14) in the Br 19—C16	521	523	524	524
v_{68}	δCOC(31) in the C1—O14—C2 + δCCC(10) in the R2	497	499	506	503
v_{69}	δCCC(18) in the C21—C20—C29 + υBrC(16) in the Br 19—C16	472	461	480	483
v_{70}	δCOC(15) in the C1—O14—C2 + δCCC(10) in the R2	454	446	455	451
v_{71}	δ CCC(26) C10—C20—C21 + γ CCCC(12) C25—C21—C10—C20	454	446	435.	435
v_{72}	γCCCC(28) in the C25—C21—C10—C20 + τCCCC(16) in the C5—C4—C3—C8 + γOCCC(14) in the O14—C2—C7—C1	414		427	425
v_{73}	τCCCC(51) in the C5—C4—C3—C8	414	403	404	405
v_{74}	δCCC(66) in the C21—C20—C29			353	355
v_{75}	γCCCC(38) in the C25—C21—C10—C20 + δCOC(10) in the C1—O14—C2			351	348
v_{76}	δCCC(30) in the C16—C4—C5 + γCCCC(17) in the C25—C21—C10—C20		327	310	332
v_{77}	τHCCC(76) in the H22—C21—C20—C25			303	309
v_{78}	δCCC(27) in the C10—C20—C21 + τHCCC(10) in the H27—C25—C20—C21			284	289
v_{79}	γCCCC(13) in the C25—C21—C10—C20 + τHCCC(10) H27—C25—C20—C21			258	259
v_{80}	τHCCC(33) in the H27—C25—C20—C21			254	243
v_{81}	δCCC(33) in the C10—C20—C29			242	242
v_{82}	τHCCC(69) in the H27—C25—C20—C21		208	218	200
v_{83}	τCCCC(22) in the C5—C4—C3—C8 + δBrCC(15) in the Br 19—C16—C4 + τCOCC(12) in the C1—O14—C2—C7 + υBrC(10) in the Br 19—C16		174	189	187
v_{84}	γCCCC(23) in the C4—C8—C2—C3 + δBrCC(11) in the Br 19—C16—C4			154	158
v_{85}	δCCC(42) in the C8—C10—C20			143	145
v_{86}	τCOCC(39) in the C1—O14—C2—C7 + γCCCC(12) in the C25—C20—C10—C8		112	122	119
v_{87}	δ BrCC(31) in the Br 19—C16—C4 + γCCCC(19) in the C25—C20—C10—C8 + τCOCC(10) in the C1—O14—C2—C7			73	74
v_{88}	τCCCC(43) in the C25—C20—C10—C8 + τCOCC(13) in the C1—O14—C2—C7 + τBrCCC(13) in the Br19—C16—C4—C3			48	51
v_{89}	τCCCC in the C25—C20—C10—C8 + τBrCCC in the Br19—C16—C4—C3			39	44
v_{90}	τCCCC in the C25—C20—C10—C8			29	22
R^2				0.9998	0.9997

υ, stretching; δ, in-plane bending; γ, out-of-plane bending; τ, torsion. [a]Potential energy distribution (PED), less than 10% are not shown. R1:ring1; R2:ring2; s: symmetric stretching; as: asymmetric stretching.

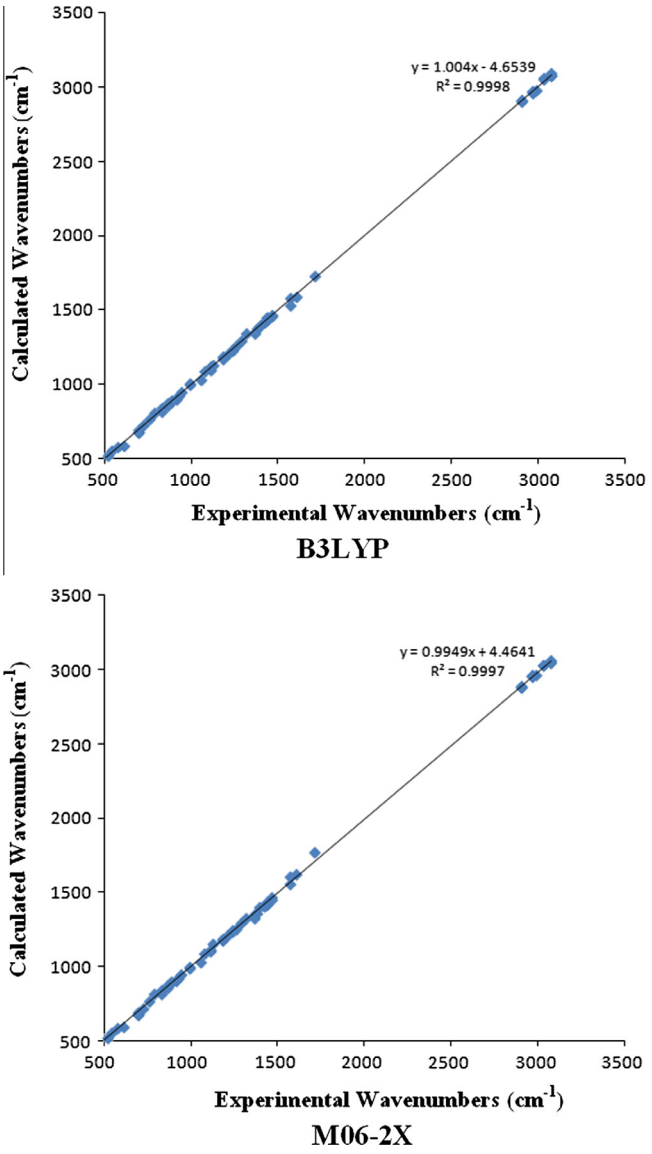

Fig. 4. Correlation graphics of experimental and theoretical (scaled) wavenumbers of the title compound.

symmetric deformations $\delta_s CH_3$ appears with an intensity varying from medium to strong and, expected in the range 1380 ± 25 cm^{-1} [30]. This band is observed at 1379(FT-IR)/1378(Ra), 1364(FT-IR)/1369(Ra) and 1364 (FT-IR) cm^{-1} in the FT-IR and Ra spectra, and calculated at 1377(B3LYP)/1359(M06-2X), 1353(B3LYP)/1349(M06-2X) and 1346(B3LYP)/1328(M06-2X) cm^{-1}, respectively. Aromatic molecules display a methyl rocking at the neighborhood 1045 cm^{-1} [30]. The second rocking in the region 970 ± 70 cm^{-1} [30] is more difficult to find among the C—H out-of-plane deformations. In the present case, these ρCH_3 modes are observed at 1181, 1113, 992 and 930 cm^{-1} in FT-IR and 1178 cm^{-1} in Raman spectra. These bands have been calculated at 1174(B3LYP)/1185(M06-2X), 1096(B3LYP)/1103(M06-2X), 1008-(B3LYP)/998(M06-2X), 1000(B3LYP)/992(M06-2X), 923(B3LYP)/927(M06-2X) and 902(B3LYP)/904(M06-2X) cm^{-1}. The methyl twisting mode is often assigned in the region 1470–1440 cm^{-1} [30]. This mode has been observed at 1435 and 1422 cm^{-1} in FT-IR spectrum, but this mode could not be observed in Raman spectrum, and calculated at 1451(B3LYP)/1437(M06-2X), 1430(B3LYP)/1411(M06-2X) and 1427(B3LYP)/1406(M06-2X) cm^{-1}. The C10-C20 stretching modes have been computed at 1236(B3LYP)/1243(M06-2X), 902(B3LYP)/904(M06-2X), 891(B3LYP)/896(M06-2X), 887(B3LYP)/889(M06-2X) and 591(B3LYP)/599(M06-2X) cm^{-1}. The related tert-butyl group vibrations have been given in Table 1. These modes are very good agreement with the theoretical spectra and our previous study [36]. This situation can be seen in Figs. 2 and 3.

C═O and C—O Vibrations

Almost all carbonyl compounds have very intense and narrow peak in the range of 1800–1600 cm^{-1} [32,37–39] or in other words the carbonyl stretching frequency has been most extensively studied by infrared spectroscopy. Coumarins have two characteristic absorption bands arising from C═O and C—O stretching vibrations. The intense C═O stretching vibrations occur at higher frequencies than that in normal ketons. This mode (C1—O15) in this study has been assigned at 1711 cm^{-1} in the FT-IR spectrum and 1708 cm^{-1} in the Raman spectrum and they are good agreement with the calculated values 1728(B3LYP)/1772(M06-2X) cm^{-1}. In Ref. [40], a very strong band at 1746 cm^{-1} in FT-IR and a strong band at 1726 cm^{-1} in FT-Raman spectra were readily assigned to the C═O vibration of coumarin; the corresponding HF and DFT computed mode is at 1808 and 1736 (82%) cm^{-1}, respectively. On the other hand in the ring 2, the computed wave numbers at 1231(B3LYP)/1238(M06-2X), 1119(B3LYP)/1116(M06-2X), 1096-(B3LYP)/1103(M06-2X), 1085(B3LYP)/1088(M06-2X), 907(B3LYP)/910(M06-2X) and 591(B3LYP)/599(M06-2X) cm^{-1} could be assigned to the C1—O14 stretching vibrations. The PEDs corresponding to these modes are 25%, 10%, 15%, 10%, 28% and 14%, respectively and show good agreement with the recorded experimental FT-IR and Raman values.

Ring system vibrations

The heteroaromatic structure shows the presence of the C—H stretching vibration in the region 3100–3000 cm^{-1} which is characteristic for the identification of the C—H stretching vibration [41,42]. For the C—H stretching vibrations we have observed the bands at 3073 and 3032 cm^{-1} in FT-IR spectrum, but these modes could not be observed in Raman spectrum. These modes have been calculated at 3095(B3LYP)/3066(M06-2X), 3080(B3LYP)/3053(M06-2X), 3078(B3LYP)/3047(M06-2X) and 3060(B3LYP)/3033(M06-2X) cm^{-1}. These modes are pure stretching modes as evident from the PED column shown in Table 1. For 8-formly-7-hydoxy-4-methyl-cumarin, the weak bands appeared at 3063 cm^{-1} in FT-IR and 3067 and 3031 cm^{-1} in FT-Raman spectra are assigned to the C—H stretching vibrations. The corresponding bands for these vibrations were calculated at 3073, 3071, and 3055 cm^{-1} in B3LYP and at 3060, 3058, and 3040 cm^{-1} in HF methods [40].

The C—H in plane bending vibration usually occurs in the region 1400–1050 cm^{-1} and the C—H out of plane bending vibrations in the range 1000–675 cm^{-1} [32,43]. In our study the C—H in plane bending vibrations have been observed at 1570(FT-IR)/1570(Ra), 1463(FT-IR), 1317(FT-IR)/1322(Ra), 1261(FT-IR), 1236(FT-IR)/1240(Ra), 1181(FT-IR)/1178(Ra), 1129(FT-IR)/1149(Ra) and 1079(FT-IR) cm^{-1}, and their corresponding theoretical values are quite compatible. These modes are numbered as 18, 19, 21, 32, 34, 36, 38, 41 and 44, respectively. The bands corresponding to the C—H in plane bending vibrations were identified in 8-formyl-7-hydroxy-4-coumarin [40] at 1248, 1228, 1184 cm^{-1} in IR and 1258 cm^{-1} in Raman spectra. The computed wave numbers at 1250, 1228, 1182 cm^{-1} and 1239, 1202, 1173 cm^{-1} by B3LYP and HF method respectively, were assigned to the C—H in plane bending vibrations. For our compound the C—H out of plane vibrations have been observed at 944(FT-IR), 868(FT-IR), 832(FT-IR) and 723(FT-IR)/728(Ra) cm^{-1}. These vibrations have been calculated

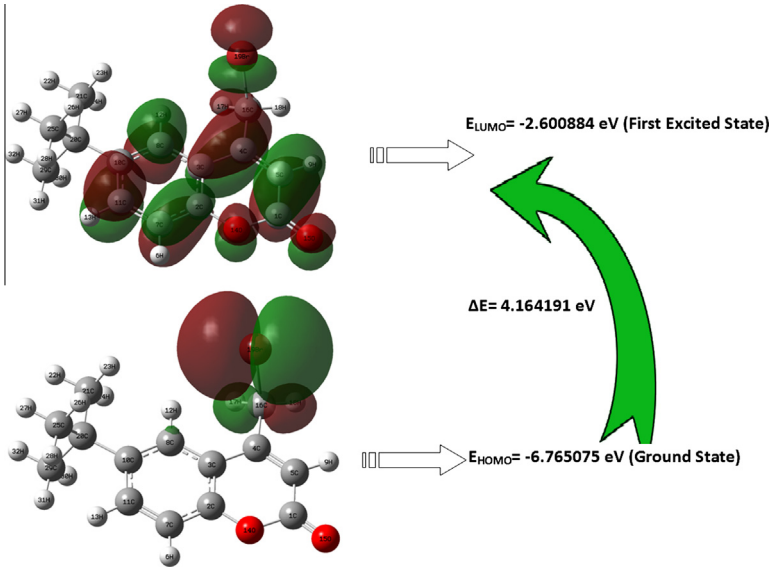

Fig. 5. Calculated HOMO–LUMO plots of the title compound.

Table 2
Comparison of HOMO–LUMO energy gaps and related molecular properties of the title compound.

Molecular properties	B3LYP/6-311++G(d,p)	M06-2X/6-311++G(d,p)
Energies (a.u)	−3267.065274	−3266.795176
E_{HOMO} (e.V)	−6.765075	−8.006741
E_{LUMO} (e.V)	−2.600884	−1.539904
Energy gap (e.V)	4.164191	6.466837
Ionization potential (I)	6.765075	8.006741
Electron affinity (A)	2.600884	1.539904
Global hardness (η)	2.082096	3.233441
Chemical potential (μ)	−4.682979	−4.773323
Electrophilicity (ψ)	5.266397	3.523276
Softness (ζ)	0.480285	0.309268
Dipol moment (debye)	5.3852	5.1852

at 946(B3LYP)/951(M06-2X), 872(B3LYP)/872(M06-2X), 857-(B3LYP)/857(M06-2X), 818(B3LYP)/818(M06-2X) and 731(B3LYP)/715(M06-2X) cm^{-1}. The out of plane bending vibrations in 8-formyl-7-hydroxy-4-methyl-coumarin [40] have been observed as medium band at 933 cm^{-1} in Raman spectrum, and the corresponding IR bands are at 929, 868 and 802 cm^{-1}, respectively.

The C—C ring stretching vibrations are expected within the region 1650–1200 cm^{-1}. In general, the bands of variable intensity are observed at 1625–1590, 1575–1590, 1470–1540, 1430–1465 and 1280–1380 cm^{-1} from the frequency ranges given by Varsanyi [44] for the five bands in the region. Most of the ring modes are altered by the substitution to aromatic ring. The actual position of these modes are determined not so much by the natural of the substituent but by the form of substitution around the ring system [33]. In Ref. [40], the frequency bands at 1595, 1480, 1184 and 1167 cm^{-1} in FT-IR and at 1594, 1484 and 1167 cm^{-1} in FT-Raman spectra were assigned to the C—C stretching vibrations for molecule 8-formyl-7-hydroxy-4-methylcoumarin. In this study, the C—C stretching modes have been observed at 1606(FT-IR)/1627(Ra), 1570(FT-IR)/1570(Ra), 1394(FT-IR) and 1289(FT-IR) cm^{-1}, and calculated at 1594(B3LYP)/1627(M06-2X), 1583-(B3LYP)/1607(M06-2X), 1535(B3LYP)/1558(M06-2X), 1396-(B3LYP)/1403(M06-2X) and 907(B3LYP)/910(M06-2X) cm^{-1}. The theoretical computed C—C—C in plane and out of plane bending vibrations by the B3LYP/6-311++G(d,p) shows good agreement with the recorded spectral data. The other wavenumbers of the ring groups such as; torsional and rocking modes are also assigned, and presented in Table 1. All these calculated values are in good agreement with the experimental data. The remainder of the observed and calculated wavenumbers and their assignments of the compound are shown in Table 1. The correlation graphic which describes harmony between the calculated and experimental wavenumbers is shown in Fig. 4. As seen from the figure, the experimental fundamentals have a good correlation at B3LYP level. The relations between the calculated and experimental wavenumbers are linear and, described by the following equations:

$$\upsilon_{Cal} = 1.004\,\upsilon_{exp} - 4.6539 \text{ at DFT/}B3LYP \text{ level}$$
$$\upsilon_{Cal} = 0.9949\,\upsilon_{exp} + 4.4641 \text{ at DFT/M06} - 2X \text{ level}$$

We have calculated R^2 values of 0.9998 at B3LYP and of 0.9997 at M06-2X levels, respectively. As a result, the performances of B3LYP and M06-2X methods in the prediction of the wavenumbers within the compound are quite close.

HOMO–LUMO analysis

Many organic compounds containing conjugated π electrons have been characterized as hyperpolarizabilities, and researched by means of vibrational spectroscopy. The π electron cloud moment from donor to acceptor can make a compound highly polarized through the single–double path when it changes from the ground state to the excited state. Both the highest occupied molecular orbital (HOMO) and the lowest unoccupied molecular orbital (LUMO) are the main orbitals taking part in chemical stability. The HOMO represents the ability to donate an electron, LUMO as an electron acceptor represents the ability to obtain an electron [45]. The LUMO and HOMO energies have been calculated at B3LYP/6-311++G(d,p) and M06-2X/6-311++G(d,p) levels, and depicted in Fig 5. Considering the chemical hardness, large HOMO–LUMO gap means a hard compound, and small HOMO–LUMO gap a soft compound. One can also relate the stability of the compound to hardness since the compound with least HOMO–LUMO gap means that it is more reactive [46]. The frontier orbitals and frontier orbital energy gap helping to exemplify the reactivity and kinetic stability of compounds are important parameters in the electronic studies [47,48]. The analysis of the wave function indicates that the electron absorption corresponding to

the transition from the ground state to the first excited state is mainly defined by one electron excitation from the highest occupied orbital (HOMO) to the lowest unoccupied orbital (LUMO) [49].

The calculated energy of the title compound is −3267.065274 a.u. at B3LYP/6-311++G(d, p) and −3266.795176 a.u. at M06-2X/6-311++G(d, p) levels. Meanwhile, the lowering of the energy gap describes that the eventual charge transfer takes place within the compound. The calculated HOMO–LUMO energy gap reflects the chemical activity of the compound, and explains the eventual charge transfer interaction within the compound, which influences its biological activity. The positive phase is represented in red color, and the negative phase in green color. The HOMO–LUMO plots are shown in Fig. 5. As seen from the figure, the HOMO is located on bromomethy and partially over the C8 atoms; the LUMO is more focused on the ring 1 and ring 2 and bromomethyl group.

In the framework of molecular orbital theory the ionization energy and electron affinity can be expressed by HOMO and LUMO orbital energies as $I = -E_{HOMO}$ and $A = -E_{LUMO}$. The global hardness is $\eta = 1/2(E_{LUMO}-E_{HOMO})$. The electron affinity can be used in combination with ionization energy to give electronic chemical potential, $\mu = 1/2(E_{LUMO} + E_{HOMO})$. The global electrophilicity index is $\psi = \mu^2/2\eta$, and softness $\zeta = 1/\eta$ [50,51]. These parameters have been evaluated and tabulated in Table 2. For coumarin and its derivatives, the HOMO–LUMO values and other related energies have been found for different similar compounds before [29,40,52].

Conclusion

In this study the vibrational analysis of a newly synthesized bacteriostatic and anti-tumor agent,4-bromomethyl-6-tert-butyl-2H-chromen-2-one compound has been studied as experimental (FT-IR and Raman spectra) and theoretical (DFT/B3LYP and DFT/M06-2X methods). The optimized geometric parameters, vibrational harmonic frequencies, PED assignments, molecular orbital energies and other properties (i.e., HOMO and LUMO energy values) of the compound have been calculated by using DFT/B3LYP and DFT/M06-2X methods with 6-311++G(d, p) basis set. The theoretical optimized geometric parameters (bond lengths, bond angles and dihedral angles) and vibrational frequencies are compared with the experimental data. Considerable level of the correlation has been noticed. The detailed PED% analyses of the compound have showed a good agreement with the experimental data. The calculated HOMO and LUMO along with their plot has been presented to understand the charge transfer occurring within the compound.

Appendix A. Supplementary material

Supplementary data associated with this article can be found, in the online version, at http://dx.doi.org/10.1016/j.molstruc.2014.09.043.

References

[1] J.D. Hepworth, C.D. Gabbut, B.N. Heron, Comprehensive Heterocyclic Chemistry, second ed., Pergamon Press, Oxford, 1996.
[2] P. O'Kennedy, R.D. Thornes (Eds.), Coumarins: Biology, Applications and Mode of Action, J. Wiley & Sons, Chichester, UK, 1997.
[3] D. Yu, M. Suzuki, L. Xie, S.L. Morris-Natschke, K.-L. Lee, Med. Res. Rev. 23 (2003) 322–345.
[4] K.M. Khan, Z.S. Saify, M.Z. Khan, M.I. Choudhary, S. Perveen, Z.H. Chohan, C.T. Supuran, Zia-Ullah Atta-Ur-Rahman, J. Enzyme Inhib. Med. Chem. 19 (2004) 373–379.
[5] C. Kontogiorgis, D.J. Hadjipavlou-Litina, Med. Chem. 48 (2005) 6400–6408.
[6] I. Kostova, Curr. Med. Chem. – Anti-Cancer Agents 5 (2005) 29–46.
[7] F. Chimenti, B. Bizzarri, A. Bolasco, D. Secci, P. Chimenti, S. Carradori, A. Granese, D. Rivanera, D. Lilli, M.M. Scaltrito, M.I. Brenciaglia, Eur. J. Med. Chem. 41 (2006) 208–212.
[8] M.V. Kulkarni, G.M. Kulkarni, C.H. Lin, C.M. Sun, Curr. Med. Chem. 13 (2006) 2795–2818.
[9] H. Madari, D. Panda, L. Wilson, R.S. Jacobs, Cancer Res. 63 (2003) 1214–1220.
[10] G. Finn, B. Creaven, D. Egan, Eur. J. Pharmacol. 481 (2003) 159–167.
[11] G. Finn, B. Creaven, D. Egan, Cancer Lett. 214 (2004) 43–54.
[12] G. Finn, B. Creaven, D. Egan, Eur. J. Pharm. Sci. 26 (2005) 16–25.
[13] C. Kontogiorgis, D. Hadjipavlou-Litina, J. Enzyme Inhib. Med. Chem. 18 (2003) 63–69.
[14] F. Bailly, C. Maurin, E. Teissier, H. Vezin, P. Cotelle, Bioorg. Med. Chem. 12 (2004) 5611–5618.
[15] T. Motai, S. Kitanaka, Chem. Pharm. Bull. (Tokyo) 52 (2004) 1215–1218.
[16] C.A. Kontogiorgis, D.J. Hadjipavlou-Litina, J. Med. Chem. 48 (2005) 6400–6408.
[17] V. Pande, M.J. Ramos, Curr. Med. Chem. 12 (2005) 357–374.
[18] K.B. Puttaraju, K. Shivashankar, V.P. Rasal, J.R. Eluru, E. Koyye, Org. Chem. Int. (2014). Article ID 297586, http://dx.doi.org/10.1155/2014/297586.
[19] H. Nagarajaiah, K.B. Puttaraju, K. Shivashankar, N.S. Begum, Acta Cryst. E69 (2013) o1056.
[20] Y. Zhao, D.G. Truhlar, Theor. Chem. Acc. 120 (2008) 215–241.
[21] A. Frish, A.B. Nielsen, A.J. Holder, Gauss View User Manual, Gaussian Inc., Pittsburg, PA, 2001.
[22] W.H. James, E.G. Buchanan, C.W. Müller, J.C. Dean, D. Kosenkov, L.V. Slipchenko, L. Guo, A.G. Reidenbach, S.H. Gellman, T.S. Zwier, J. Phys. Chem. A115 (2011) 13783–13798.
[23] M.J. Frisch, G.W. Trucks, H.B. Schlegel, G.E. Scuseria, M.A. Robb, J.R. Cheeseman, J.A. Montgomery, T. Vreven, K.N. Kudin, J.C. Burant, J.M. Millam, S.S. Iyengar, J. Tomasi, V. Barone, B. Mennucci, M. Cossi, G. Scalmani, N. Rega, G.A. Petersson, H. Nakatsuji, M. Hada, M. Ehara, K. Toyota, R. Fukuda, J. Hasegawa, M. Ishida, T. Nakajima, Y. Honda, O. Kitao, H. Nakai, M. Klene, X. Li, J.E. Knox, H.P. Hratchian, J.B. Cross, V. Bakken, C. Adamo, J. Jaramillo, R. Gomperts, R.E. Stratmann, O. Yazyev, A.J. Austin, R. Cammi, C. Pomelli, J.W. Ochterski, P.Y. Ayala, K. Morokuma, G.A. Voth, P. Salvador, J.J. Dannenberg, V.G. Zakrzewski, S. Dapprich, A.D. Daniels, M.C. Strain, O. Farkas, D.K. Malick, A.D. Rabuck, K. Raghavachari, J.B. Foresman, J.V. Ortiz, Q. Cui, A.G. Baboul, S. Clifford, J. Cioslowski, B.B. Stefanov, G. Liu, A. Liashenko, P. Piskorz, I. Komaromi, R.L. Martin, D.J. Fox, T. Keith, M.A. Al-Laham, C.Y. Peng, A. Nanayakkara, M. Challacombe, P.M.W. Gill, B. Johnson, W. Chen, M.W. Wong, C. Gonzalez, J.A. Pople, Gaussian 03, Revision D.01, Gaussian Inc., Wallingford, 2004.
[24] M.H. Jamróz, Vibrational Energy Distribution Analysis VEDA 4, Warsaw, 2004.
[25] M.H. Jamróz, Spectrochim. Acta A 114 (2013) 220–230.
[26] H.-K. Fun, J.H. Goh, D. Wu, Y. Zhang, Acta Cryst. E67 (2011) o136.
[27] R. Gowda, M. Basanagouda, M.V. Kulkarni, K.V.A. Gowda, Acta Cryst. E66 (2011) o2906.
[28] V. Sortur, J. Yenagi, J. Tonannavar, V.B. Jadhav, M.V. Kulkarni, Spectrochim. Acta A 71 (2008) 688–694.
[29] J. Tonannavar, J. Yenagi, V. Sortur, V.B. Jadhav, M.V. Kulkarni, Spectrochim. Acta A 77 (2010) 351–358.
[30] N.P.G. Roeges, A Guide to the Complete Interpretation of Infrared Spectra of Organic Structures, Wiley, New York, 1994.
[31] N.B. Colthup, L.H. Daly, S.E. Wiberly, Introduction to Infrared and Raman Spectroscopy, third ed., Academic Press, Boston, 1990.
[32] G. Socrates, Infrared Characteristic Group Frequencies, John Wiley, GB, 1980.
[33] L.J. Bellamy, The Infrared Spectra of Complex Molecules, Capman and Hall, London, 1975.
[34] D. Mahadevan, S. Periandy, Spectrochim. Acta A 78 (2011) 575–581.
[35] E.F. Mooney, Spectrochim. Acta 20 (6) (1964) 1021–1025.
[36] Y. Sert, L.M. Singer, M. Findlater, H. Doğan, Ç. Çırak, Spectrochim. Acta A 128 (2014) 46–53.
[37] V. Krishnakumar, R.J. Xavier, Indian J. Pure Appl. Phys. 41 (2003) 597–601.
[38] A. Prabakaran, S. Muthu, Spectrochim. Acta A 118 (2014) 578–588.
[39] R. Meenakshi, J. Lakshmi, S. Gunesakaran, S. Srinivasan, Mol. Simul. 36 (2010) 425–433.
[40] H. Moghanian, A. Mobinikhaledi, R. Monjezi, J. Mol. Struct. 1052 (2013) 135–145.
[41] R.M. Silverstein, F.X. Webster, Spectroscopic Identification of Organic Compound, sixth ed., John Willey & Sons, New York, 1998.
[42] V.K. Rastogi, M.A. Palafox, R.P. Tanwar, L. Mittal, Spectrochim. Acta A 58 (2002) 1987–2004.
[43] B.C. Smith, Infrared Spectral Interpretation: A Systematic Approach, CRC Press, Boca Raton, Florida, 1998.
[44] G. Varanyi, Vibrational Spectra of Benzene Derivatives, Academic Press, New York, 1969.
[45] E. Kavitha, N. Sundaraganesan, S. Sebastian, M. Kurt, Spectrochim. Acta A 77 (2010) 612–619.
[46] K. Chaitanya, Spectrochim. Acta A 86 (2012) 159–173.
[47] E. Kavitha, N. Sundaraganesan, S. Sebastian, Indian J. Pure Appl. Phys. 48 (2010) 20–30.
[48] A. Jayaprakash, V. Arjunan, S. Mohan, Spectrochim. Acta A 81 (2011) 620–630.
[49] S. Subashchandrabose, H. Saleem, Y. Erdogdu, G. Rajarajan, V. Thanikachalam, Spectrochim. Acta A 82 (2011) 260–269.
[50] T. Vijayakumar, I. Hubert Joe, C.P.R. Nair, V.S. Jayakumar, Chem. Phys. 343 (2008) 83–99.
[51] M. Govindarajan, M. Karabacak, A. Suvitha, S. Periandy, Spectrochim. Acta A 89 (2012) 137–148.
[52] N.U. Sri, K. Chaitanya, M.V.S. Prasad, V. Veeraiah, A. Veeraiah, Spectrochim. Acta A 97 (2012) 728–736.